Wang et al. *Zool. Res.* 2025, 46(3): 634−646
https://doi.org/10.24272/j.issn.2095-8137.2024.348
https://cstr.cn/32248.14.zr.2024.348

ZR | Zoological Research

Article Open Access

Transcriptomic profiling of cardiac development in Bama Xiang pigs across key developmental stages

Sheng-Nan Wang[1], Wen-Jie Tian[1], Deng-Ke Pan[2], Tang Hai[3], Yue-Hui Ma[1], Dan-Dan Wang[1,*], Lin Jiang[1,*]

[1] *State Key Laboratory of Animal Biotech Breeding*, *Institute of Animal Sciences*, *Chinese Academy of Agricultural Sciences (CAAS)*, *Beijing* 100193, *China*

[2] *Institute of Organ Transplantation*, *Sichuan Academy of Medical Sciences* & *Sichuan Provincial People's Hospital*, *Chengdu*, *Sichuan* 610072, *China*

[3] *State Key Laboratory of Stem Cell and Reproductive Biology*, *Institute of Zoology*, *Chinese Academy of Sciences*, *Beijing* 100101, *China*

ABSTRACT

Pigs have emerged as valuable large-animal models for cardiac xenotransplantation; however, the temporal dynamics of myocardial development in this species remains insufficiently defined. This study analyzed gene expression patterns across four key developmental stages (neonatal, juvenile, sexual maturity, and adulthood) to delineate the molecular mechanisms driving porcine myocardial development. Increases in heart weight were accompanied by proportional expansion of myocardial fiber area and chamber size, reflecting coordinated structural development. Transcriptomic profiling of myocardial tissue by RNA sequencing (RNA-seq) identified 2 189 differentially expressed genes (DEGs) across stage comparisons. Short time-series expression miner (STEM) analysis classified these DEGs into four major expression clusters enriched in pathways associated with myocardial development, immune responses, cell proliferation, and metabolic processes. Among 359 DEGs conserved across all developmental stages, six candidate genes were strongly associated with myocardial development. Reverse transcription-quantitative real-time polymerase chain reaction (RT-qPCR) confirmed a significant correlation between the expression of these candidate genes and myocardial development in porcine tissue. These findings establish a transcriptomic framework for porcine myocardial maturation and provide a molecular basis for advancing cardiac xenotransplantation.

Keywords: Cardiac tissue; Bama Xiang pig; Multiple stages; Heart development; Transcriptomics

This is an open-access article distributed under the terms of the Creative Commons Attribution Non-Commercial License (http://creativecommons.org/licenses/by-nc/4.0/), which permits unrestricted non-commercial use, distribution, and reproduction in any medium, provided the original work is properly cited.

Copyright ©2025 Editorial Office of Zoological Research, Kunming Institute of Zoology, Chinese Academy of Sciences

INTRODUCTION

The heart is the first organ to attain functionality during embryogenesis and is shaped by a range of genetic and environmental factors. While murine models have provided foundational insights into the molecular basis of cardiac diseases, their clinical translational relevance is constrained by fundamental anatomical and physiological disparities with humans. In contrast, large mammalian models offer considerable advantages. Among these, pigs are a particularly valuable reference in clinical studies due to their close resemblance to humans in cardiovascular hemodynamics and anatomical structures (Yoshida & Yamanaka, 2017). Pigs have proven instrumental in modeling diabetic cardiomyopathy and cardiovascular diseases (Richter & Hinkel, 2021), offering mechanistic insights and platforms for therapeutic testing. Beyond disease modeling, pigs are central to the advancement of organ xenotransplantation. Landmark studies have demonstrated the feasibility of orthotopic cardiac transplantation using genetically modified pig hearts, achieving a survival period of 945 days in non-human primates (Längin et al., 2018). More recently, xenotransplantation has seen a significant breakthrough in clinical application: in 2022, a patient survived for two months following pig-to-human heart transplantation (Mohiuddin et al., 2023), followed in 2023 by successful transplantation in two brain-dead recipients with sustained cardiac function post-surgery (Moazami et al., 2023), and subsequently, a second living human recipient (Anand et al., 2023). Pigs have also been utilized for xenotransplantation of kidneys and livers, further underscoring their clinical relevance. Among pig breeds, the Bama Xiang pig (*Sus scrofa*), a miniature breed native to China, has been selectively bred for over two decades, resulting in a genetically stable population with consistent physiological traits. This breed exhibits high reproductive efficiency and notable similarities to humans in organ morphology, biochemical profiles, physiological functions, and disease susceptibility, making it an ideal model for investigating cardiac development and advancing

Received: 02 March 2025; Accepted: 08 May 2025; Online: 15 May 2025
Foundation items: This work was supported by the National Natural Science Foundation of China (32222079 to L.J. and 32202621 to D.D.W.)
*Corresponding authors, E-mail: wangdd1993@126.com; jianglin@caas.cn

xenotransplantation studies (Liu et al., 2008).

Extensive multi-omics investigations have been conducted on pig cardiac tissue, offering valuable insights into heart development. Notably, porcine cardiomyocytes retain mitotic potential between two and six months postnatally, during which multiple gene networks associated with growth and differentiation remain transcriptionally active (Velayutham et al., 2020). High-throughput approaches, such as RNA sequencing (RNA-seq), have revealed transcriptional changes in neonatal Yorkshire-Landrace pigs during their first two weeks of life (Ye et al., 2018; Zhu et al., 2018). Complementing these findings, Bai et al. (2023) integrated transcriptomic and chromatin accessibility profiling (ATAC-seq) in female Berkshire×Xizang hybrid pigs at 1 day, 28 days, and 6 months of age, thereby enhancing the temporal resolution of gene regulatory dynamics. Similarly, Schachtschneider et al. (2015) characterized both the transcriptomic and DNA methylation landscapes in myocardial tissue from 3-year-old Duroc pigs. Additionally, Zhu et al. (2022) generated epigenomic datasets spanning prenatal to postnatal stages in Bama Xiang pigs and Large White pigs. Despite these advances, research on cardiac development has largely focused on isolated or limited time points (Takeuchi et al., 2011), with a lack of systematic studies on key pathways and stages across the developmental spectrum. Integrative, multi-omics investigations that capture the dynamic progression of cardiac development across multiple stages remain scarce, leaving gaps in our understanding of the full trajectory of heart development.

Advancements in high-throughput next-generation sequencing (NGS) have become a powerful tool in mammalian research (Ghosh et al., 2015; Huang et al., 2017; Zhang et al., 2017), enabling studies on the genetic regulation of heart development. In humans, large-scale single-cell transcriptomic and epigenomic datasets (Vanoudenhove et al., 2020) have provided unprecedented resolution of cellular heterogeneity within the embryonic (Asp et al., 2019; Cui et al., 2019; Farah et al., 2024) and adult heart (Litviňuková et al., 2020; Tucker et al., 2020; Wang et al., 2020), identifying lineage-specific markers and potential regulatory axes involved in cardiac regeneration. Complementary studies using induced pluripotent stem cell-derived cardiomyocytes (iPS-CMs) have demonstrated that, after four weeks of culture, these cells acquire gene expression profiles and structural features resembling those of adult cardiomyocytes (Yang et al., 2022), offering an *in vitro* model to elucidate the temporal dynamics of cardiac maturation (Ronaldson-Bouchard et al., 2018). Murine models have further elucidated conserved molecular trajectories in cardiac ontogeny. Single-cell sequencing from embryonic day 10.5 (E10.5) to postnatal day 9 (P9) has mapped distinct cellular and molecular signatures across cardiac cell populations during key transitional windows (Feng et al., 2022). The down-regulation of regeneration-associated genes such as *Bex1* and *Bex4* by postnatal day 21 (P21) coincides with the loss of proliferative capacity in cardiomyocytes, highlighting critical inflection points in postnatal cardiac maturation (Delaughter et al., 2016). Multi-omics analyses across 10 developmental stages, from E10.5 to postnatal week 8 (8w), have further delineated the orchestration of gene regulatory networks underlying mouse cardiac development and maturation (Gu et al., 2022). Other studies have demonstrated that modulating postnatal expression of cardiomyocyte cell-cycle regulators can enhance the regenerative capacity of mouse hearts (Jiang et al., 2022; Mahmoud et al., 2013). In rats, single-cell RNA-seq on postnatal days 1 and 7 revealed a pivotal role for AP-1 in regulating postnatal cardiomyocyte maturation (Zhang et al., 2023a). Together, these studies have utilized transcriptomic and epigenomic platforms to explore the genetic regulation of heart development, identifying key pathways and genes and offering valuable insights for advancing regenerative strategies and improving our understanding of cardiac developmental biology.

Substantial advances have been made in elucidating the molecular mechanisms of heart development in both humans and mice. However, studies on human cardiac maturation face sampling limitations, making it difficult to comprehensively investigate heart development from the neonatal period to adulthood. Moreover, key differences in cardiac anatomy, physiology, and disease progression between humans and mice limit the translational applicability of murine models (Rao et al., 2022). In contrast, pigs exhibit developmental timelines and cardiac features that closely resemble those of humans, offering a biologically relevant platform for modeling human heart development. For instance, porcine postnatal day 5 (P5) corresponds to the human neonatal nursing period, 3 months post-birth (3 mon) approximates early childhood, 5 months post-birth (5 mon) aligns with adolescence (sexual maturity), and 8 months post-birth (8 mon) represents adulthood. In this study, high-throughput RNA-seq was employed to map dynamic gene expression changes across myocardial development in Bama Xiang pigs across four critical stages, including neonatal, juvenile, sexually mature, and adult. Comprehensive transcriptome analysis revealed dynamic gene expression trajectories and identified key candidate genes associated with myocardial growth and development. These findings provide a valuable molecular framework for understanding cardiac developmental processes in a physiologically relevant large-animal model and support the refinement of strategies for pig-to-human cardiac xenotransplantation.

MATERIALS AND METHODS

Laboratory animals

All animals used in this study were female Bama Xiang pigs sourced from the Chinese Academy of Sciences Changping Experimental Base (Beijing, China) to ensure a consistent genetic background. Individuals were randomly selected at four key developmental stages: P5, 3 mon, 5 mon, and 8 mon, with sample sizes of five, three, five, and three individuals, respectively. All animals were housed in the same environment with free access to food and water under uniform conditions and controlled temperature, humidity, and ventilation to ensure optimal living conditions. Regular health assessments were conducted throughout the study to ensure the well-being and suitability of each pig for subsequent analyses. All animal experiments were conducted in accordance with the regulations and guidelines established by the Animal Care Committee of the Beijing Academy of Agricultural Sciences, adhering to established animal welfare protocols (No. IAS2 019-60).

Sacrifice and sample collection

Cardiac tissue samples were obtained from female Bama

Xiang pigs at four defined developmental stages (P5, 3 mon, 5 mon, and 8 mon). All procedures were conducted in strict compliance with institutional animal welfare guidelines. Prior to euthanasia, precise body weights were recorded. Pigs were anesthetized via overdose of an approved anesthetic agent, ensuring humane sacrifice. Hearts were rapidly excised following cessation of circulation, with care taken to minimize tissue damage and maintain sample integrity. Immediately after isolation, whole-heart weights were measured. The epicardium and endocardium were carefully removed, and samples of left ventricular muscle tissues were dissected for downstream analyses. Each myocardial sample was divided into two portions: one was fixed in 4% paraformaldehyde (G1 101, Servicebio, China) for histological analysis, and the other was rapidly frozen in liquid nitrogen for RNA extraction and molecular biology experiments.

Ultrasound examination of the heart

Cardiac function was evaluated using transthoracic echocardiography on 6-month-old (6 mon), 8.5-month-old (8.5 mon), and 12-month-old (12 mon) Bama Xiang pigs. Prior to examination, animals underwent a 12 h fasting period. Sedation was induced by intramuscular administration of an appropriate dose of anesthetic, after which the pigs were positioned on the operating table. The left thoracic area was shaved to expose the skin, and anesthesia was maintained with a mixture of isoflurane and medical-grade oxygen via a ventilator. Upon stabilization of vital parameters, echocardiographic imaging was performed using a Philip CX50 ultrasound system (Philips Healthcare, Netherlands). Cardiac structural and functional indices, including left ventricular internal dimensions at end-diastole (LVIDd), left ventricular internal dimensions at end-systole (LVIDs), ejection fraction (EF), and fractional shortening (FS), were measured to quantify myocardial performance. All examinations were performed by experienced professionals to ensure measurement accuracy and data reliability for comprehensive assessment of developmental changes in cardiac function.

Histological analysis of cardiac muscle fiber sections

Myocardial tissue samples were fixed in 4% paraformaldehyde (G1 101, Servicebio, China), processed using a paraffin-embedding system, and sectioned at a uniform thickness of 4 μm using a precision microtome (Leica Microsystems, Germany). Histological analyses included hematoxylin and eosin (H&E) staining, wheat germ agglutinin (WGA) immunofluorescence staining, and Masson's trichrome staining. Morphological observations were performed under a Nikon microscope (Nikon, Japan) to assess myocardial fiber morphology, structural integrity, and fibrotic deposition. For each specimen, five randomly selected fields of view were observed. Quantification of myocardial fiber cross-sectional area and collagen fiber content was performed using Image Pro Plus software (v.6.0).

RNA extraction and quality control

RNA extraction was performed on liquid nitrogen-frozen myocardial tissue samples using Trizol reagent (R711-02, Vazyme, China), with 2–3 mg of tissue taken from each sample in strict accordance with the manufacturer's protocols. RNA concentration and purity were measured using a NanoDrop 1000 spectrophotometer (Thermo Fisher Scientific, USA). RNA integrity was assessed through gel electrophoresis and further quantified using an Agilent 2100 bioanalyzer (Agilent Technologies, USA). Only RNA samples meeting stringent quality control criteria (total yield≥2.0 μg, RIN>7.0) were retained for subsequent transcriptomic analysis.

RNA-seq and detection of differentially expressed genes (DEGs)

RNA libraries were prepared using a standard Illumina platform library construction kit. The mRNA was purified from total RNA using polyT, then fragmented into 300–350 bp fragments. The fragmented RNA was reverse-transcribed into cDNA, followed by end repair, A-tail addition, junction ligation, and polymerase chain reaction (PCR) amplification to generate the final library. Library quality was assessed prior to high-throughput sequencing on the Illumina Nova6 000 platform (Illumina, USA), generating at least 9 Gb of clean data per sample. RNA-seq reads were aligned to the Ensembl Sscrofa11.1 reference genome using Hisat2 (v.2.0.4) (Kim et al., 2019) with default parameters. Uniquely mapped reads were counted using featureCount (https://github.com/topics/featureCount) (Liao et al., 2014) and differential expression analysis was conducted using DESeq2 (Love et al., 2014). Genes exhibiting a $|\log_2(\text{fold change})| \geq 1$ and Q-value≤0.05 were designated as DEGs.

Hierarchical cluster and correlation analysis of transcriptomic profiles

Principal component analysis (PCA) was conducted to reduce the dimensionality of gene expression data across all myocardial samples using the "ggfortify" package in R (v.4.4.1, http://cran.r-project.org/). Pearson correlation coefficients between all sample pairs were computed via the base "stats" package in R. Hierarchical cluster analysis of all expressed genes was performed using the clustering function in the "pheatmap" package in R. The optimal number of clusters was determined by calculating the Calinski-Harabasz index, allowing genes with similar expression trajectories to be grouped. Hierarchical clustering and STEM analysis was performed using the "TCseq" package in R.

Transcription factor identification and functional enrichment analysis

DEGs were analyzed for functional annotation and pathway enrichment using the g:Profiler database (http://biit.cs.ut.ee/gprofiler/) (Raudvere et al., 2019). Significantly enriched Gene Ontology (GO) terms and Kyoto Encyclopedia of Genes and Genomes (KEGG) pathways were identified using a g:SCS adjusted P-value threshold of <0.05. Visualization of enriched terms was performed using relevant R packages.

Gene Set Enrichment Analysis (GSEA) was conducted using the *c2.cp.kegg_legacy.v2024.1.Hs.symbols.gmt* and *c5.all.v2024.1.Hs.symbols.gmt* gene sets from the Molecular Signatures Database (MSigDB) with GSEA software (v.4.0.3) (Subramanian et al., 2005). Pairwise comparisons between each developmental stage were used to identify significantly enriched gene sets (false discovery rate (FDR) Q<0.05). GSEA visualization tools were used to generate enrichment plots and heatmaps to illustrate the enrichment of key gene sets.

Reverse transcription-quantitative real-time PCR (RT-qPCR)

To validate transcriptomic findings, RT-qPCR was employed to confirm the expression of selected DEGs. Gene-specific primers were designed based on reference sequences, and

cDNA templates were obtained by reverse transcription using HiScript III All-in-one RT SuperMix Perfect (R433-01, Vazyme, Nanjing, China) according to the manufacturer's instructions. RT-qPCR was conducted using Taq Pro Universal SYBR qPCR Master Mix (Q712-03, Vazyme, China) on a QuantStudio™ 7 Flex system (Thermo Fisher Scientific, USA). Each sample was analyzed in triplicate to ensure experimental reproducibility. *β-actin* and *GAPDH* were used as internal reference genes for normalization. Relative gene expression was quantified using the $2^{-\Delta\Delta Ct}$ method (Livak & Schmittgen, 2001). Primer sequences are listed in Supplementary Table S1.

Statistical analysis

All statistical analyses were performed using GraphPad Prism software (v.8.3). Results are presented as mean±standard error of the mean (SEM) from at least three biological replicates. Comparisons between groups were made using unpaired Student's *t*-tests. Error bars denote SEM, with significance levels set to: ***: $P<0.001$, **: $P<0.01$, and *: $P<0.05$.

RESULTS

Heart weight and heart-to-body weight ratio increase with developmental stage

The sampling time points selected represented four distinct stages of porcine development (Figure 1A): P5 (suckling period), 3 mon (adolescence), 5 mon (sexual maturity), and 8 mon (adulthood). Quantitative assessment of heart weight and the heart-to-body weight ratio (HW/BW) revealed stage-dependent changes (Figure 1B; Supplementary Table S2). Heart weight exhibited a significant upward trajectory across developmental stages. At P5, the average heart weight was approximately 8 g, markedly lower than at 5 mon (90 g) and 8 mon (100 g) ($P<0.001$). Additionally, heart weight at 8 mon was significantly higher than at 5 mon ($P<0.05$).

In contrast, the HW/BW ratio showed a declining trend with age (Figure 1C; Supplementary Table S2). The highest ratio was observed at P5 (1.3%), which was significantly greater than the ratio at 5 mon (0.6%) and 8 mon (0.4%) ($P<0.001$).

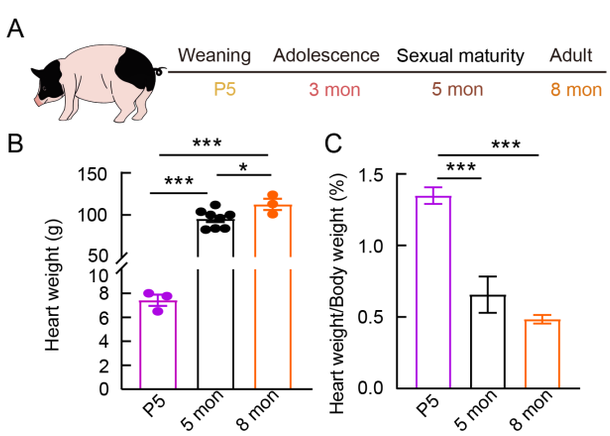

Figure 1 Changes in heart weight across four developmental stages

A: Description of sampling time points and corresponding developmental stages. B: Changes in heart weight (g) across different time points, *n*=3:7:3. C: Changes in HW/BW (%) (heart-to-body weight ratio) across different time points. Results are presented as mean±SEM, *: $P<0.05$; ***: $P<0.001$.

However, the reduction in heart ratio between 5 mon and 8 mon was not statistically significant. These findings suggest that while heart weight increased significantly with development, the proportion of heart mass relative to body weight decreased.

Changes in myocardial fiber area and heart chamber size

Histological and immunofluorescent analyses revealed pronounced structural remodeling of myocardial tissue across developmental stages. Notably, H&E staining of myocardial sections (Figure 2A) showed that myocardial fibers were small and loosely arranged at P5, but fiber area gradually increased with advancing age, reaching a more mature morphology by 5 mon and 8 mon. These findings were further supported by WGA immunofluorescence staining (Figure 2B). Quantitative analysis revealed a significant and progressive increase in myocardial fiber cross-sectional area from P5 to 5 mon. Fiber area at P5 was significantly smaller than at 3 mon, with further enlargement occurring between 3 mon and 8 mon ($P<0.001$). Although fiber area continued to increase at 8 mon, the difference between 5 mon and 8 mon was not statistically significant (Figure 2C, D; Supplementary Table S2).

These histological changes paralleled the physiological remodeling observed through transthoracic echocardiography. Measurements of LVIDd and LVIDs revealed an age-dependent increase between 6 mon and 12 mon. LVIDd increased significantly over this period, while the change in LVIDs was not statistically significant (Figure 2E; Supplementary Table S2). Collectively, these results confirm that myocardial fiber hypertrophy and chamber expansion are key features of postnatal cardiac maturation in Bama Xiang pigs, mirroring the patterns of heart weight gain observed across developmental stages.

Absence of fibrosis and cardiac failure

Myocardial fibrosis was quantified by Masson's trichrome staining. Representative histological images (Figure 3A) revealed varying degrees of fibrosis across all developmental stages. Quantitative analysis indicated that the area of cardiac fibrosis fluctuated from P5 to 8 mon, although the overall trend was not significant (Figure 3B). To further assess myocardial function, EF and FS were measured at 6 mon, 8.5 mon, and 12 mon. Both EF and FS values remained stable across time points, with no significant differences detected (Figure 3C; Supplementary Table S2). These findings indicate that structural expansion of the myocardium in Bama Xiang pigs during postnatal development occurs as an adaptive, non-pathological process, and does not result in cardiac dysfunction or fibrosis, hallmarks of pathological hypertrophy.

RNA-seq and analysis

High-throughput RNA-seq yielded at least 9 Gb of clean data per sample following stringent quality control. The Q20 and Q30 quality scores exceeded 94.72% and 88.46%, respectively, and GC content ranged from 45% to 50.70% (Supplementary Table S3). On average, over 89.09% of clean reads mapped successfully to the reference genome (Supplementary Table S4), confirming the suitability of the dataset for comprehensive transcriptomic analysis.

Gene expression levels across all samples were quantified using fragments per kilobase of transcript per million mapped fragments (FPKM). Most genes exhibited low or negligible expression (FPKM<1), with only a fraction showing high transcriptional activity—a distribution pattern consistent with

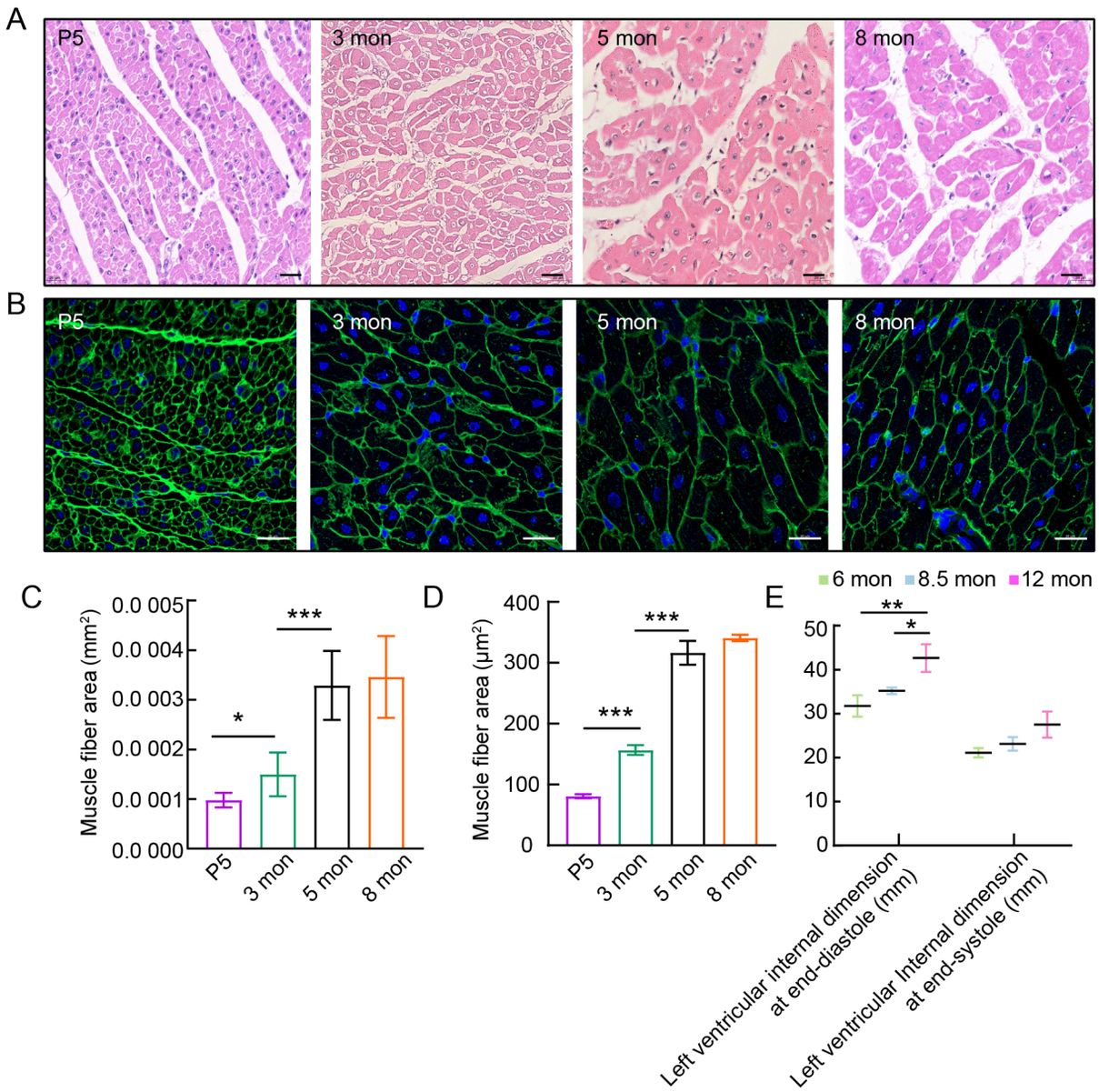

Figure 2 Myocardial fiber structure and size across developmental stages

A: Hematoxylin and eosin (H&E) staining of myocardial fibers at postnatal day 5 (P5), 3 months post-birth (3 mon), 5 months post-birth (5 mon), and 8 months post-birth (8 mon). Scale bars: 20 μm. B: Wheat germ agglutinin (WGA) immunofluorescence staining of myocardial fibers (green) and nuclei (blue) at the same stages. Scale bars: 20 μm. C: Quantification of cardiomyocyte size analyzed by H&E staining. D: Quantification of cardiomyocyte size analyzed by WGA immunofluorescence staining. E: Left ventricular internal dimension at end-diastole (LVIDd) and left ventricular internal dimension at end-systole (LVIDs) at 6-months-old (6 mon), 8.5-months-old (8.5 mon), and 12-months-old (12 mon), n=3:3:7. Results are presented as mean±SEM, *: P<0.05; **: P<0.01; ***: P<0.001.

transcriptomic datasets in mammalian tissues (GTEx Consortium, 2017; Wolf et al., 2023) (Figure 4A, B). PCA revealed distinct clustering of samples according to developmental stage (Figure 4C). PC1, which accounted for 77.45% of the variance, effectively separated 8 mon samples from earlier time points. PC2 distinguished 5 mon samples from P5 and 3 mon, which clustered more closely, suggesting transcriptomic similarity in the early postnatal period. Heatmap analysis supported the PCA results, with samples from each developmental stage forming a distinct cluster (Supplementary Figure S1A), with samples from P5 and 3 mon separating from the same large branch. Correlation analysis (Figure 4D) further confirmed this pattern. Notably, intra-group correlations were consistently high (approaching 1.0), reflecting strong reproducibility, while inter-group correlations were lower. Among the cross-stage comparisons, the correlation between P5 and 3 mon was higher than that observed between any other pair of time points, consistent with their close clustering.

Identification of DEGs during heart development

DEGs were identified between consecutive developmental stages using stringent thresholds of $|\log_2(\text{fold change})| \geq 1$ and Q-value≤0.05. Pairwise comparisons between time points revealed substantial transcriptional reprogramming during cardiac maturation. Specifically, 2 126, 2 593 and 6 344 DEGs were screened between P5 and 3 mon, 3 mon and 5 mon, and 5 mon and 8 mon, respectively (Figure 5A; Supplementary Figure S1B–D and Table S5), including 895, 1 003, and 3 517 up-regulated genes and 1 231, 1 590, and 2 827 down-regulated genes. The smallest number of DEGs was observed

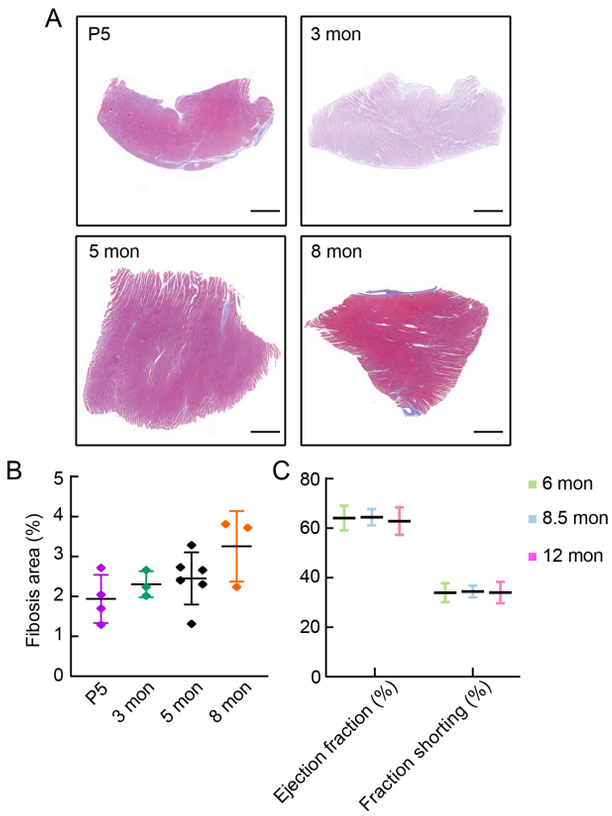

Figure 3 Fibrosis area and cardiac function

A: Representative Masson's trichrome staining of heart sections. Fibrotic areas were stained blue. Scale bars: 500 μm. B: Quantification of fibrosis area (%) at different developmental stages. C: Cardiac function as measured by ejection fraction (EF) and fraction shortening (FS) at 6-months-old (6 mon), 8.5-months-old (8.5 mon), and 12-months-old (12 mon), *n*=3:3:7.

between P5 and 3 mon, consistent with the cluster analysis results that showed high transcriptomic similarity between these two stages. In contrast, the highest number of DEGs was found between 5 mon and 8 mon, which was likely due to the fact that 5 mon to 8 mon is a period from sexual maturity to adulthood. This period likely involves the activation and suppression of numerous genes to support late-stage cardiac maturation, including adjustments in metabolic, structural, and regulatory pathways necessary for adult myocardial function.

STEM-based hierarchical clustering and transcription factor analysis

To elucidate coordinated gene expression dynamics during cardiac development, STEM analysis was performed on the combined set of 2 189 DEGs identified across three developmental transitions. Hierarchical clustering, guided by the Calinski-Harabasz index, grouped these genes into four distinct temporal expression profiles (Figure 5B). The four clusters contained 1 020, 458, 455, and 255 DEGs, respectively, with cluster K1 accounting for 46.6% of all DEGs. Time series analysis revealed distinct developmental expression trajectories for each cluster, highlighting stage-specific transcriptional programs (Figure 5C).

To identify key transcriptional regulators associated with each cluster, transcription factor analysis was conducted using relevant databases. Transcription factor diversity for each cluster was calculated as: (number of transcription factors in each cluster/number of genes in the cluster)×100 (Figure 5D). Cluster K1 exhibited the highest number of transcription factors (*n*=51), including the cardiac-specific transcription factor Nkx2.5. Cluster K3 exhibited the highest transcription factor diversity value (5.49%) and included T-box family members TBX18 and TBX20, both of which play critical roles in cardiac development. Additional clusters also demonstrated distinct transcriptional regulatory profiles. Cluster K2 was associated with transcription factors FOS, LHX9, and NOBOX, while cluster K4 was regulated by transcription factors ATOHB, PITX3, and SOX18.

Functional enrichment analysis of DEGs

To investigate the biological significance of temporally clustered gene sets, functional enrichment analysis was performed for each cluster using g:Profiler, with a g:SCS adjusted *P*-value<0.05 used as the threshold for significance. The top 10 significantly enriched terms and pathways for each cluster are presented in Supplementary Figure S2A–D, with the remaining terms listed in Supplementary Table S6. Cluster K1, which contained the largest number of genes, exhibited the broadest functional enrichment, showing significant enrichment for terms directly associated with cardiac and muscle development (Figure 5E). Genes in cluster K2 were primarily enriched in disease and immune-related pathways, such as "Rheumatoid arthritis". Genes in cluster K3 were predominantly enriched in mitosis and cell proliferation-related pathways, including "Mitotic cell cycle" and "Regulation of cell cycle". Genes in cluster K4 were mainly enriched in terms related to mitochondrial energy metabolism and cellular metabolism, including the "Mitochondrion organization" and "Oxidative phosphorylation" pathways.

To complement these findings, GSEA was performed on DEGs from each pairwise developmental comparison using an FDR *Q*-value<0.05 as the threshold for significance. This analysis provided detailed insights into the functional enrichment of DEGs and identified core genes involved in pathways related to myocardial development. During the P5 to 3 mon transition, two muscle development-related pathways, including "GOCC_CONTRACTILE_MUSCLE_FIBER" and "GOBP_STRIATED_MUSCLE_CELL_DEVELOPMENT", were significantly up-regulated at 3 mon (Supplementary Figure S3). Concurrently, pathways related to cell division, including "GOBP_CELL_DIVISION" and "GOBP_MITOTIC_CELL_CYCLE_PROCESS", were significantly down-regulated at P5. Between 3 mon and 5 mon, metabolism-related pathways were significantly down-regulated, indicating a metabolic shift in cardiac tissue during this period. In contrast, the transition from 5 mon to 8 mon was characterized by a marked up-regulation in metabolism-related pathways at 8 mon and a significant down-regulation in mitosis and cell cycle-related pathways at 5 mon. A comprehensive list of enriched pathways and associated gene sets is provided in Supplementary Table S7.

Systematic identification and validation of candidate genes

Venn diagrams were constructed to visualize the overlap of DEGs at the three developmental intervals: P5 to 3 mon, 3 mon to 5 mon, and 5 mon to 8 mon. A total of 359 genes were differentially significant across the three comparisons (Figure 6A). Visualization of their expression trajectories (Figure 6B) revealed a unique transcriptional pattern. Notably, gene expression from 3 mon to 5 mon displayed an inverse trend relative to the P5 to 3 mon and 5 mon to 8 mon stages.

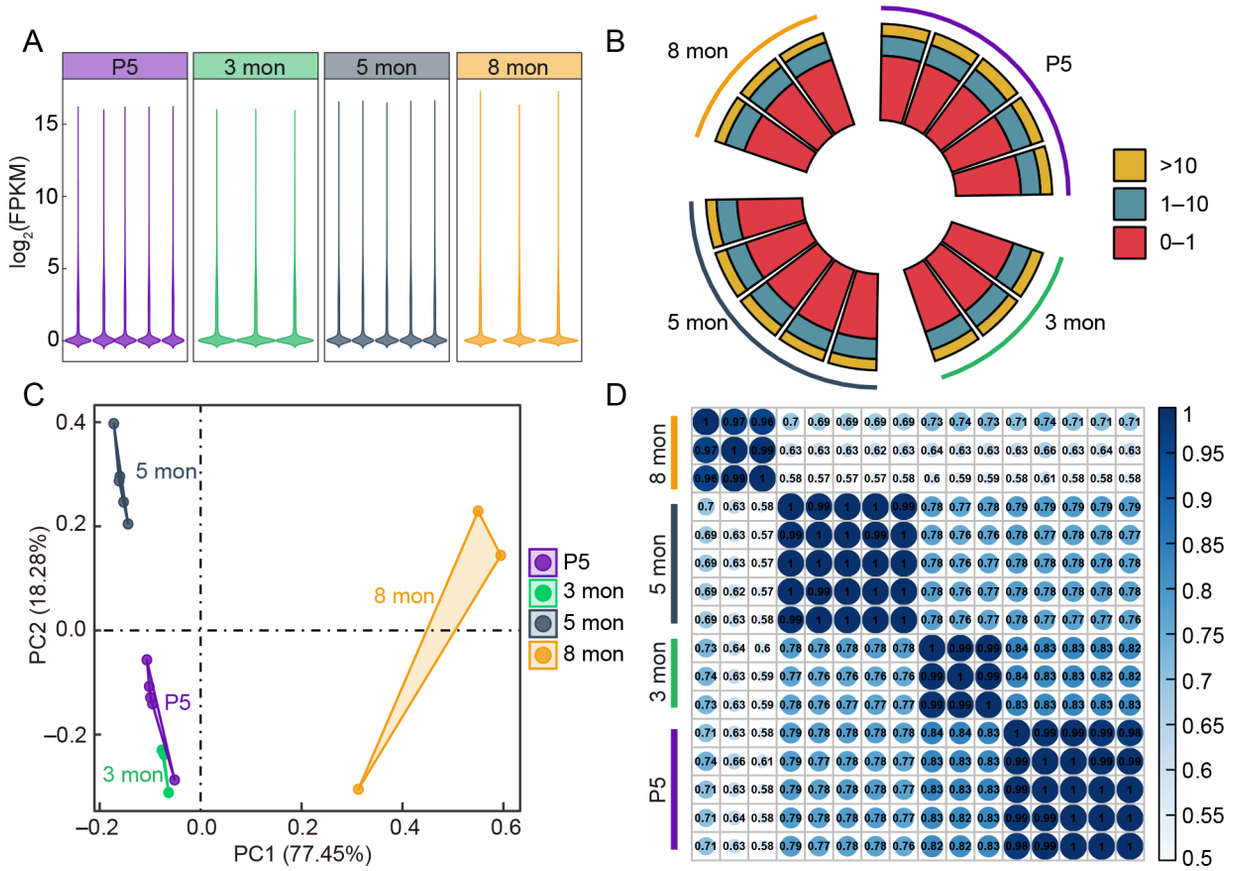

Figure 4 Transcriptomic data analysis

A: Violin plots showing distribution of gene expression, with vertical axis representing $\log_2$(FPKM) values of each sample. B: Circular dendrogram showing relationship among genes across four time points. Color coding represents fold-change expression levels, with red indicating fold-change between 0 and 1, blue indicating fold-change between 1 and 10, and yellow indicating fold-change greater than 10. C: Principal component analysis (PCA) plot showing separation of samples from four developmental stages along PC1 and PC2, which explained 77.45% and 18.28% of the variance, respectively. Purple represents samples from P5 individuals, green represents samples from 3 mon individuals, black represents samples from 5 mon individuals, and orange represents samples from 8 mon individuals. D: Correlation heatmap showing pairwise correlations of gene expression, with darker blue indicating higher correlation. Number within each circle denotes correlation value between two individuals.

This distinct shift suggests that the 3 mon to 5 mon interval may represent a critical transitional window in myocardial development, potentially involving a regulatory inflection point or reorganization of developmental signaling programs. GO enrichment analysis of the 359 shared DEGs identified 33 genes significantly enriched in terms associated with cardiac development, including "Cardiac cell development", "Cardiocyte differentiation", and "Heart development" (Figure 6C). The term "Muscle structure development" was the most enriched, with 27 of the 33 genes annotated to this category. An UpSet plot was used to illustrate the overlap among enriched GO terms, identifying eight DEGs that were significantly enriched in all seven cardiac-related terms (Figure 6D).

Expression profiling of these 33 genes across developmental stages (Figure 7A) showed divergent trends between gene clusters. Genes assigned to cluster K1 were up-regulated during transitions from P5 to 3 mon and 5 mon to 8 mon, but down-regulated between 3 mon and 5 mon. In contrast, genes in cluster K3 exhibited the opposite trend. Among the eight DEGs significantly enriched in all seven cardiac development GO terms, six belonged to cluster K1 and two (*TBX18* and *PDGFRA*) belonged to cluster K3. Notably, six of these eight genes, based on both transcription factor enrichment and literature evidence, were correlated with cardiomyocyte development and were thus regarded as candidate regulators of myocardial maturation in Bama Xiang pigs. Validation by RT-qPCR confirmed the transcriptomic expression patterns of these six candidate genes, particularly across the P5 to 3 mon and 3 mon to 5 mon stages, illustrating the accuracy and reliability of the results (Figure 7B).

DISCUSSION

Cardiac growth in Bama Xiang pigs was marked by a progressive increase in both heart weight and myocardial fiber area with advancing age (Figures 1, 2). However, the heart-to-body weight ratio exhibited a downward trend, indicating a relative slowdown in cardiac growth compared to overall body mass. As the pigs matured, the growth of other tissues, particularly skeletal muscle, outpaced that of the heart, leading to a stabilization of heart size while body weight continued to increase. In the later stages of development, the internal diameter of the ventricular chamber showed enlargement (Figure 2E), consistent with findings in Dorper lambs from birth to 120 days (Aleixo et al., 2022). This expansion represents a common physiological adaptation that allows the heart to accommodate the increasing circulatory demands of a growing body.

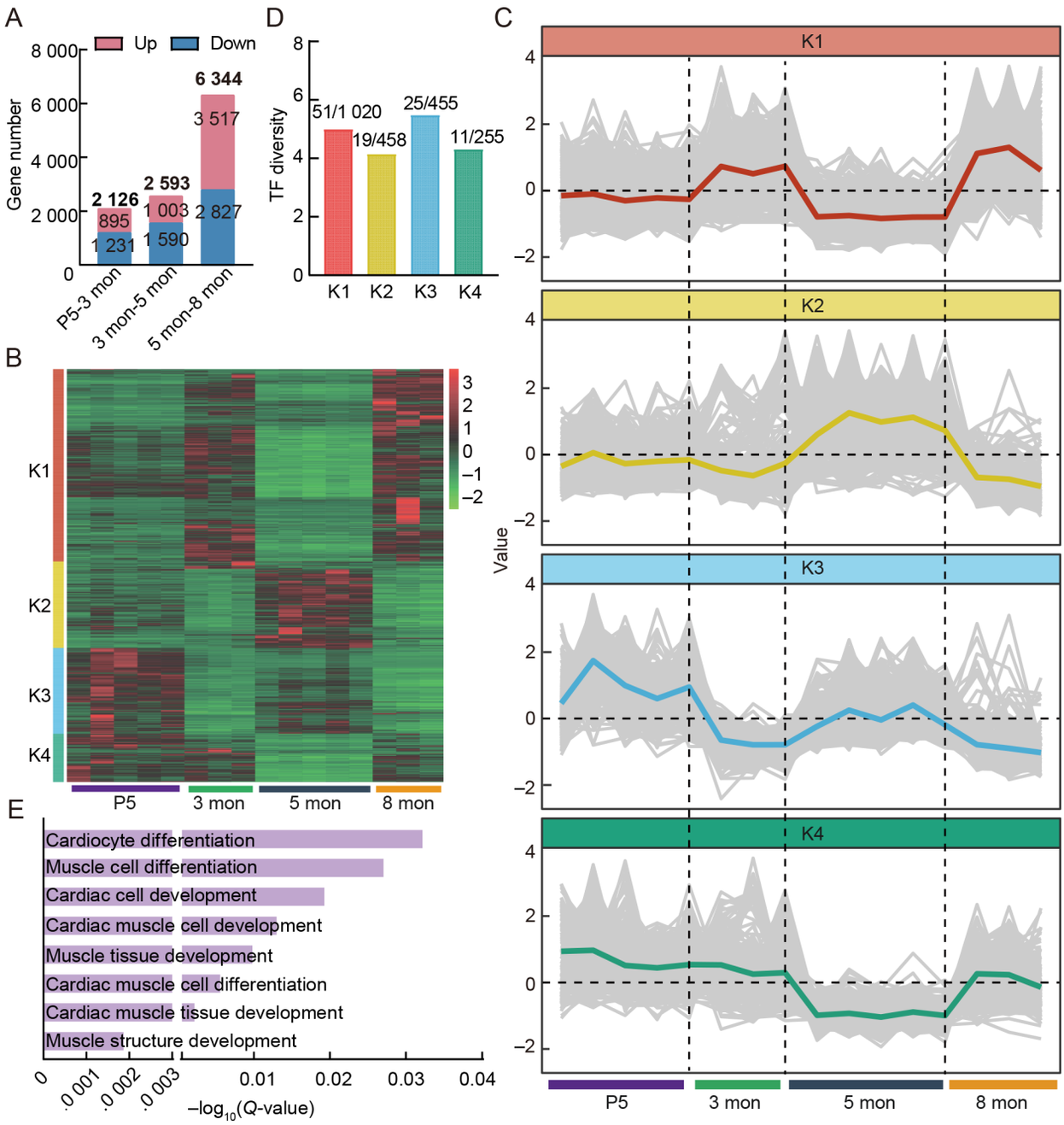

Figure 5 Short time-series expression miner (STEM) clustering analysis and transcription factor prediction

A: Bar plot showing number of up-regulated (red) and down-regulated (blue) differentially expressed genes (DEGs) across pairwise comparisons of developmental stages (P5–3 mon, 3 mon–5 mon, and 5 mon–8 mon). Number in each colored box represents number of genes contained within. B: Heatmap based on STEM analysis showing expression profiles of DEGs across four developmental stages (P5, 3 mon, 5 mon, and 8 mon). DEGs were partitioned into four clusters (K1 to K4), with red indicating up-regulation and green indicating down-regulation. Four colors on vertical axis represent the four gene clusters, while four colors on horizontal axis represent the four sample collection time points. C: Time course expression trends for each cluster (K1–K4), with solid lines representing average expression of genes in each cluster and gray lines representing individual gene expression trends. D: Transcription factor (TF) diversity for each cluster, TF diversity=(number of TFs in each cluster/number of genes in the cluster)×100. Numbers on top of each bar indicate total number of transcription factors and genes in each cluster. E: Gene Ontology (GO) enrichment analysis of cluster K1 genes, showing enrichment in pathways related to cardiac and muscle development. Horizontal axis represents $-\log_{10}(Q\text{-value})$ of each term.

Cardiac hypertrophy is broadly classified into physiological and pathological forms, each characterized by distinct structural and functional signatures (Nakamura & Sadoshima, 2018). Physiological hypertrophy arises during growth and maturation and is defined by preserved or enhanced cardiac output without fibrotic or inflammatory remodeling. In contrast, pathological hypertrophy is characterized by increased fibrosis, impaired cardiac function, heart failure, and elevated mortality (Bernardo et al., 2010). Myocardial fibrosis is a common metric used to evaluate fibrosis severity and potential pathological changes in the heart. In the present study, although myocardial fibrosis showed a mild upward trend with age, the changes were not statistically significant. As part of normal heart development, moderate proliferation of

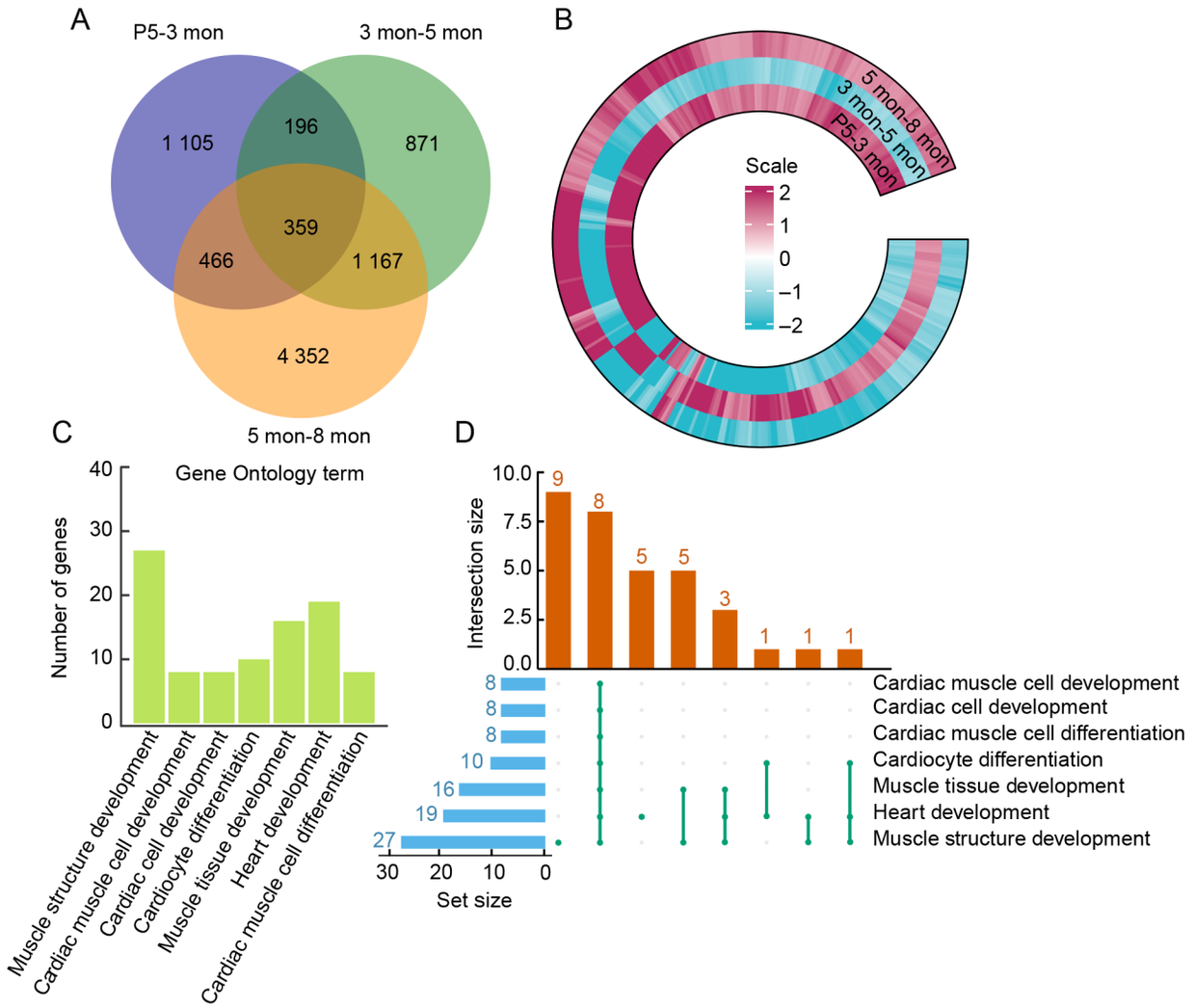

Figure 6 Candidate gene screening

A: Venn diagram showing overlap of differentially expressed genes (DEGs) across three pairwise comparisons: P5–3 mon, 3 mon–5 mon, and 5 mon–8 mon. Number within each circle represents number of genes shared between each intersection. B: Circular heatmap showing overlapping DEGs from three comparisons, with color intensity representing gene expression levels ($\log_2$(fold change)), where red indicates up-regulation and blue indicates down-regulation. C: Gene Ontology (GO) enrichment analysis of overlapping DEGs, showing enrichment in terms related to cardiac and muscle development. Vertical axis represents number of genes enriched each term. D: UpSet plot showing intersection size of genes enriched in various GO terms in (C). Blue bar chart represents total number of genes in each term, orange bar chart represents number of genes contained in different intersections. Markers and connecting lines illustrate overlap between various gene sets.

fibroblasts and expansion of connective tissue accompany cardiomyocyte growth. Importantly, this low-level fibrosis did not impair cardiac function, as evidenced by stable EF and FS on echocardiographic assessment (Figure 3C). These findings suggest that the heart undergoes a physiological hypertrophic response during development, supporting increased circulatory demand without compromising function.

Transcriptomic profiling demonstrated that samples from P5 and 3 mon clustered closely, indicating that these stages share a similar gene expression landscape and correspond to the early phase of cardiac development in Bama Xiang pigs (Figure 4C, D). In contrast, the transition from 5 mon to 8 mon yielded the highest number of DEGs among the four developmental stages (Figure 5A), despite the absence of significant changes in myocardial fiber area during this interval (Figure 2C, D). This discrepancy suggests that the 5 to 8 month period represents a functional rather than morphological shift, marking the transition from sexual maturity to early adulthood. This stage is likely driven by metabolic remodeling, including increased reliance on fatty acid oxidation and reduced glucose utilization, which are key features of cardiomyocyte maturation and bioenergetic adaptation (Supplementary Table S6).

Previous studies have suggested that the PPAR signaling pathway is crucial in regulating cardiac energy metabolism during hypertrophic growth (Lehman & Kelly, 2002). In 30-day old mice, over 80% of cardiomyocyte energy is derived from fatty acid oxidation, while glycolysis accounts for less than 7%, indicating a metabolic shift from glycolytic to oxidative metabolism (Lopaschuk & Jaswal, 2010). In the early stages of cardiac development (P5 to 3 mon), cardiomyocyte development in Bama Xiang pigs was characterized predominantly by cardiomyocyte proliferation, with DEGs showing enrichment in cell cycle regulation and mitotic activity. As development progressed from juvenile to sexual maturity (3 mon to 5 mon), cardiomyocyte hypertrophy became the primary driver of cardiac maturation. During this phase, myocardial energy metabolism underwent substantial

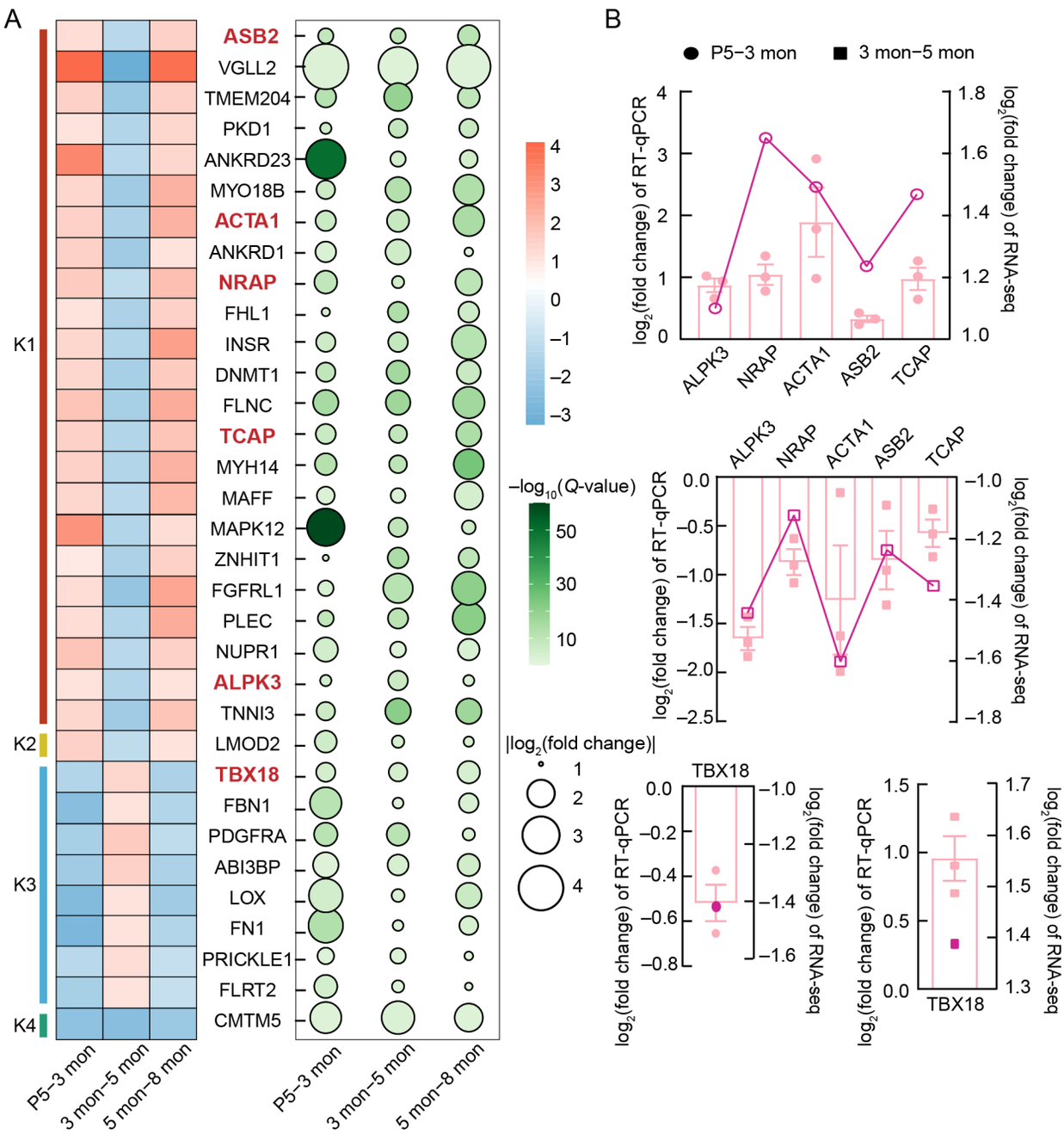

Figure 7 Expression patterns and validation of candidate genes involved in cardiac development

A: Heatmap (left) showing expression levels (log_2(fold change)) of candidate genes across three developmental comparisons (P5–3 mon, 3 mon–5 mon, and 5 mon–8 mon) for clusters K1–K4. Red indicates up-regulation and blue indicates down-regulation. Circle plot (right) shows significance ($–log_{10}$Q-value) of each gene, with circle size representing fold change and circle color representing Q-value significance (darker green indicates more significant). B: Reverse transcription-quantitative real-time polymerase chain reaction (RT-qPCR) validation of selected candidate genes. Left y-axis shows log_2(fold change) of RT-qPCR results, right y-axis shows log_2(fold change) from RNA-seq data for comparison. Data are presented for P5–3 mon and 3 mon–5 mon comparisons.

maturation, transitioning toward oxidative capacity, although some residual proliferative activity remained detectable (Supplementary Table S6). These findings are consistent with the conclusions of Velayutham et al. (2020).

STEM-based temporal clustering and functional enrichment analyses revealed that genes within the K1 cluster were progressively up-regulated throughout development and significantly enriched in pathways associated with myocardial and muscle development. These genes were also regulated by the cardiac-specific transcription factor Nkx2.5, a master regulator of heart development. As one of the earliest transcription factors expressed in the vertebrate heart, Nkx2.5 plays a critical role in cardiac morphogenesis (Lee et al., 1998, 2004), promoting both cardiomyocyte proliferation and differentiation (Jiang et al., 2020; Zhou et al., 2022). The expression trajectory of K1 genes suggests their involvement in hypertrophic expansion of primary myocardial fibers during postnatal development. In contrast, genes in cluster K3 exhibited a consistent down-regulation trend from birth to adulthood and were predominantly enriched in pathways associated with mitosis and cell proliferation, consistent with the decline in cardiomyocyte proliferation. In pigs, with a

gestation period of approximately 3.7 months, the first two weeks after birth are characterized by simultaneous cardiomyocyte proliferation and hypertrophic growth. During this period, increases in cardiomyocyte length, left ventricular mass, and nuclear content reflect a transitional phase in which both cellular expansion and division contribute to myocardial development. In contrast, in pigs older than 6 months, cardiomyocytes exhibit pronounced elongation and a substantial increase in multinucleation (Zhu et al., 2018). Together, these findings support the conclusion that proliferation-associated genes dominate early development, characterized by significant up-regulation, whereas myocardial development-related genes primarily regulate later stages.

Six key genes implicated in porcine myocardial development were identified through co-localization across different pairwise comparisons. Five of these genes (*ASB2*, *ACTA1*, *NRAP*, *TCAP*, and *ALPK3*) were grouped in cluster K1, showing significant up-regulation at 3 mon but marked down-regulation at 5 mon (Figure 7B; Supplementary Figure S4). This down-regulation may reflect a relative deceleration in myocardial growth during the transition to sexual maturity, although histological and morphometric data confirmed ongoing cardiomyocyte hypertrophy at 5 mon (Figure 2).

GSEA provided further insights into the functional roles of these DEGs. In the P5 to 3 mon comparison, two muscle development-related pathways were significantly enriched at 3 mon, with *TCAP*, *ASB2*, *ACTA1*, and *NRAP* identified as core components (Supplementary Figure S3). Similarly, *ACTA1*, *ALPK3*, and *TCAP* were significantly enriched in two myocardial-related pathways, “Hypertrophic cardiomyopathy” and “Abnormal myocardium morphology”. Notably, none of these candidate genes were enriched in pathways associated with cell cycle regulation, mitosis, or energy metabolism, suggesting their primary function lies in modulating cardiomyocyte hypertrophy rather than influencing proliferative activity or metabolic remodeling.

These genes are essential for maintaining cardiac structure and muscle contraction. *ASB2* and *NRAP*, in particular, are essential for the assembly and maintenance of myofibrils (Lu & Horowits, 2008; Manisastry et al., 2009). In *Asb2* knockout mice, severe disruption of myofibril organization leads to a rapid decline in cardiac efficiency, culminating in embryonic lethality (Métais et al., 2018). Similarly, in zebrafish, *Asb2* knockout causes significant thinning of the ventricular wall and dilation of cardiac chambers (Min et al., 2021). Mechanistically, *ASB2* interacts with key transcription factors, such as Smad9, to maintain cardiac morphology and regulate heart development, and also modulates Tbx2 expression (Singh et al., 2009). Loss-of-function mutations in *NRAP* impair normal cardiac development and function, leading to pericardial edema and disorganized cardiomyocyte alignment (Zhang et al., 2023b). Furthermore, nonsense mutations of *NRAP* can lead to cardiac dysfunction in humans, likely due to its specific expression at the junction of cardiac intercalated disks and skeletal muscle tendons (Truszkowska et al., 2017).

TCAP and *ALPK3* encode sarcomeric proteins that localize to the Z-line and M-band, respectively, where they play critical roles in maintaining the structural integrity of the contractile apparatus, and therefore myocardial contraction and relaxation (Zhang et al., 2009). Disruption of these proteins causes myomesin misalignment, ultimately compromising cardiomyocyte structure and function (Agarwal et al., 2022). In zebrafish, knockout of *Tcap* disrupts cardiac regeneration and inhibits cardiomyocyte proliferation, while also inducing elevated reactive oxygen species (ROS) levels and enhanced mitochondrial autophagy (Zhao et al., 2024). *ALPK3* is critically involved in cardiomyocyte differentiation. Overexpression of *Alpk3* in P19CL6 cells has been shown to enhance their differentiation into cardiomyocytes (Hosoda et al., 2001), underscoring its function in early cardiac lineage specification.

The *ACTA1* gene encodes skeletal muscle α-actin, a key structural protein required for sarcomere assembly, muscle contraction, and early cardiomyocyte development. Its expression is tightly regulated by transcription factors such as serum response factor (SRF), which ensure proper sarcomere formation (Niu et al., 2008). In addition to transcriptional control, *ACTA1* is also subject to post-transcriptional regulation by microRNAs; for instance, *miR-26b* has been shown to suppress *ACTA1* expression, thereby affecting cardiomyocyte hypertrophy (Sowa et al., 2012). In response to external stimuli, such as angiotensin II, *ACTA1* and other hypertrophy-related genes show significantly increased expression (Bartoli et al., 2022). This up-regulation causes structural and functional abnormalities in cardiomyocytes, altering cell size and function and exacerbating cardiac hypertrophy and fibrosis (Cañes et al., 2020).

TBX18, a member of the T-box family transcription factor family and part of cluster K3, emerged as a key candidate gene associated with porcine myocardial development. *TBX18* is a key regulator of pacemaker cell development, orchestrating the formation, proliferation, and differentiation of the sinoatrial node (Wiese et al., 2009). Alongside *TBX18*, other genes in cluster K3 are regulated by TBX20, another critical T-box factor involved in cardiac morphogenesis. TBX20 functions cooperatively with transcriptional regulators such as Nkx2.5, GATA4, and GATA5 to regulate cardiac gene expression across multiple cardiac cell lineages. Furthermore, TBX20 plays a pivotal role in coordinating cell proliferation, differentiation, and chamber formation (Brown et al., 2005; Stennard et al., 2005), as well as promoting cardiomyocyte proliferation and survival. TBX20 is also critical for the formation and maintenance of heart valves (Cai et al., 2005; Shelton & Yutzey, 2007; Singh et al., 2005).

In summary, transcriptomic profiling of myocardial tissue from Bama Xiang pigs —an indigenous Chinese miniature breed—across neonatal, juvenile, sexually mature, and adult stages identified a dynamic landscape of DEGs associated with cardiac development. Co-localization and functional enrichment analyses revealed a set of candidate genes likely to regulate key phases of myocardial maturation. This study provides a valuable molecular resource for understanding porcine cardiac development and highlights genes with potential relevance for future applications in xenotransplantation. These key genes may serve as potential targets for genome editing aimed at advancing cardiac organ transplantation and cardiovascular disease research.

DATA AVAILABILITY

The sequencing data obtained in this study have been uploaded to the Science Data Bank database (SDB, Data DOI: 10.57 760/sciencedb.20 204), Genome Sequence Archive database (GSA, accession number PRJCA036 145), and National Center for Biotechnology Information database (NCBI, BioProjectID PRJNA663 759).

SUPPLEMENTARY DATA

Supplementary data to this article can be found online.

COMPETING INTERESTS

The authors declare that they have no competing interests.

AUTHORS' CONTRIBUTIONS

L.J. conceived and designed the experiments. L.J. and D.D.W. revised the manuscript. S.N.W. performed the experiments and wrote the manuscript. S.N.W. and W.J.T. analyzed the data. Y.H.M., D.K.P., and T.H. contributed to sample collection. All authors read and approved the final version of the manuscript.

REFERENCES

Agarwal R, Wakimoto H, Paulo JA, et al. 2022. Pathogenesis of cardiomyopathy caused by variants in *ALPK3*, an essential pseudokinase in the cardiomyocyte nucleus and sarcomere. *Circulation*, **146**(22): 1674–1693.

Aleixo ASC, Ferreira DOL, Tsunemi MH, et al. 2022. Influence of Dorper lamb development from birth to 120 days of age on clinical and echocardiographic parameters. *Scientific Reports*, **12**(1): 19726.

Anand RP, Layer JV, Heja D, et al. 2023. Design and testing of a humanized porcine donor for xenotransplantation. *Nature*, **622**(7982): 393–401.

Asp M, Giacomello S, Larsson L, et al. 2019. A spatiotemporal organ-wide gene expression and cell atlas of the developing human heart. *Cell*, **179**(7): 1647–1660. e19.

Bai JY, Lin Y, Zhang JM, et al. 2023. Profiling of chromatin accessibility in pigs across multiple tissues and developmental stages. *International Journal of Molecular Sciences*, **24**(13): 11076.

Bartoli F, Evans EL, Blythe NM, et al. 2022. Global PIEZO1 gain-of-function mutation causes cardiac hypertrophy and fibrosis in mice. *Cells*, **11**(7): 1199.

Bernardo BC, Weeks KL, Pretorius L, et al. 2010. Molecular distinction between physiological and pathological cardiac hypertrophy: experimental findings and therapeutic strategies. *Pharmacology & Therapeutics*, **128**(1): 191–227.

Brown DD, Martz SN, Binder O, et al. 2005. Tbx5 and Tbx20 act synergistically to control vertebrate heart morphogenesis. *Development*, **132**(3): 553–563.

Cai CL, Zhou WL, Yang L, et al. 2005. T-box genes coordinate regional rates of proliferation and regional specification during cardiogenesis. *Development*, **132**(10): 2475–2487.

Cañes L, Martí-Pàmies I, Ballester-Servera C, et al. 2020. Neuron-derived orphan receptor-1 modulates cardiac gene expression and exacerbates angiotensin II-induced cardiac hypertrophy. *Clinical Science*, **134**(3): 359–377.

Cui YL, Zheng YX, Liu XX, et al. 2019. Single-cell transcriptome analysis maps the developmental track of the human heart. *Cell Reports*, **26**(7): 1934–1950. e5.

DeLaughter DM, Bick AG, Wakimoto H, et al. 2016. Single-cell resolution of temporal gene expression during heart development. *Developmental Cell*, **39**(4): 480–490.

Farah EN, Hu RK, Kern C, et al. 2024. Spatially organized cellular communities form the developing human heart. *Nature*, **627**(8005): 854–864.

Feng W, Bais A, He HT, et al. 2022. Single-cell transcriptomic analysis identifies murine heart molecular features at embryonic and neonatal stages. *Nature Communications*, **13**(1): 7960.

Ghosh M, Sodhi SS, Song KD, et al. 2015. Evaluation of body growth and immunity-related differentially expressed genes through deep RNA sequencing in the piglets of Jeju native pig and Berkshire. *Animal Genetics*, **46**(3): 255–264.

GTEx Consortium. 2017. Genetic effects on gene expression across human tissues. *Nature*, **550**(7675): 204–213.

Gu YY, Zhou Y, Ju SH, et al. 2022. Multi-omics profiling visualizes dynamics of cardiac development and functions. *Cell Reports*, **41**(13): 111891.

Hosoda T, Monzen K, Hiroi Y, et al. 2001. A novel myocyte-specific gene *Midori* promotes the differentiation of P19CL6 cells into cardiomyocytes. *Journal of Biological Chemistry*, **276**(38): 35978–35989.

Huang WL, Guo YT, Du WH, et al. 2017. Global transcriptome analysis identifies differentially expressed genes related to lipid metabolism in Wagyu and Holstein cattle. *Scientific Reports*, **7**(1): 5278.

Jiang FQ, Liu K, Chen JX, et al. 2022. Mettl3-mediated m6A modification of Fgf16 restricts cardiomyocyte proliferation during heart regeneration. *elife*, **11**: e77014.

Jiang WF, Xu YJ, Zhao CM, et al. 2020. A novel TBX5 mutation predisposes to familial cardiac septal defects and atrial fibrillation as well as bicuspid aortic valve. *Genetics and Molecular Biology*, **43**(4): e20200142.

Kim D, Paggi JM, Park C, et al. 2019. Graph-based genome alignment and genotyping with HISAT2 and HISAT-genotype. *Nature Biotechnology*, **37**(8): 907–915.

Längin M, Mayr T, Reichart B, et al. 2018. Consistent success in life-supporting porcine cardiac xenotransplantation. *Nature*, **564**(7736): 430–433.

Lee KH, Evans S, Ruan TY, et al. 2004. SMAD-mediated modulation of YY1 activity regulates the BMP response and cardiac-specific expression of a GATA4/5/6-dependent chick *Nkx2.5*enhancer. *Development*, **131**(19): 4709–4723.

Lee Y, Shioi T, Kasahara H, et al. 1998. The cardiac tissue-restricted homeobox protein Csx/Nkx2.5 physically associates with the zinc finger protein GATA4 and cooperatively activates atrial natriuretic factor gene expression. *Molecular and Cellular Biology*, **18**(6): 3120–3129.

Lehman JJ, Kelly DP. 2002. Gene regulatory mechanisms governing energy metabolism during cardiac hypertrophic growth. *Heart Failure Reviews*, **7**(2): 175–185.

Liao Y, Smyth GK, Shi W. 2014. featureCounts: an efficient general purpose program for assigning sequence reads to genomic features. *Bioinformatics*, **30**(7): 923–930.

Litviňuková M, Talavera-López C, Maatz H, et al. 2020. Cells of the adult human heart. *Nature*, **588**(7838): 466–472.

Liu Y, Zeng BH, Shang HT, et al. 2008. Bama miniature pigs (*Sus scrofa domestica*) as a model for drug evaluation for humans: comparison of in vitro metabolism and in vivo pharmacokinetics of lovastatin. *Comparative Medicine*, **58**(6): 580–587.

Livak KJ, Schmittgen TD. 2001. Analysis of relative gene expression data using real-time quantitative PCR and the $2^{-\Delta\Delta CT}$ Method. *Methods*, **25**(4): 402–408.

Lopaschuk GD, Jaswal JS. 2010. Energy metabolic phenotype of the cardiomyocyte during development, differentiation, and postnatal maturation. *Journal of Cardiovascular Pharmacology*, **56**(2): 130–140.

Love MI, Huber W, Anders S. 2014. Moderated estimation of fold change and dispersion for RNA-seq data with DESeq2. *Genome Biology*, **15**(12): 550.

Lu SJ, Horowits R. 2008. Role of nonmuscle myosin IIB and N-RAP in cell spreading and myofibril assembly in primary mouse cardiomyocytes. *Cell Motility and the Cytoskeleton*, **65**(9): 747–761.

Mahmoud AI, Kocabas F, Muralidhar SA, et al. 2013. Meis1 regulates postnatal cardiomyocyte cell cycle arrest. *Nature*, **497**(7448): 249–253.

Manisastry SM, Zaal KJM, Horowits R. 2009. Myofibril assembly visualized by imaging N-RAP, alpha-actinin, and actin in living cardiomyocytes. *Experimental Cell Research*, **315**(12): 2126–2139.

Métais A, Lamsoul I, Melet A, et al. 2018. Asb2α-Filamin A axis is essential for actin cytoskeleton remodeling during heart development. *Circulation Research*, **122**(6): e34–e48.

Min KD, Asakura M, Shirai M, et al. 2021. ASB2 is a novel E3 ligase of SMAD9 required for cardiogenesis. *Scientific Reports*, **11**(1): 23056.

Moazami N, Stern JM, Khalil K, et al. 2023. Pig-to-human heart xenotransplantation in two recently deceased human recipients. *Nature Medicine*, **29**(8): 1989–1997.

Mohiuddin MM, Singh AK, Scobie L, et al. 2023. Graft dysfunction in compassionate use of genetically engineered pig-to-human cardiac xenotransplantation: a case report. *The Lancet*, **402**(10399): 397–410.

Nakamura M, Sadoshima J. 2018. Mechanisms of physiological and pathological cardiac hypertrophy. *Nature Reviews: Cardiology*, **15**(7): 387–407.

Niu ZY, Iyer D, Conway SJ, et al. 2008. Serum response factor orchestrates nascent sarcomerogenesis and silences the biomineralization gene program in the heart. *Proceedings of the National Academy of Sciences of the United States of America*, **105**(46): 17824–17829.

Rao KS, Kameswaran V, Bruneau BG. 2022. Modeling congenital heart disease: lessons from mice, hPSC-based models, and organoids. *Genes & Development*, **36**(11-12): 652–663.

Raudvere U, Kolberg L, Kuzmin I, et al. 2019. g: Profiler: a web server for functional enrichment analysis and conversions of gene lists (2019 update). *Nucleic Acids Research*, **47**(W1): W191–W198.

Richter C, Hinkel R. 2021. Research('s) sweet hearts: experimental biomedical models of diabetic cardiomyopathy. *Frontiers in Cardiovascular Medicine*, **8**: 703355.

Ronaldson-Bouchard K, Ma SP, Yeager K, et al. 2018. Advanced maturation of human cardiac tissue grown from pluripotent stem cells. *Nature*, **556**(7700): 239–243.

Schachtschneider KM, Madsen O, Park C, et al. 2015. Adult porcine genome-wide DNA methylation patterns support pigs as a biomedical model. *BMC Genomics*, **16**(1): 743.

Shelton EL, Yutzey KE. 2007. Tbx20 regulation of endocardial cushion cell proliferation and extracellular matrix gene expression. *Developmental Biology*, **302**(2): 376–388.

Singh MK, Christoffels VM, Dias JM, et al. 2005. *Tbx20* is essential for cardiac chamber differentiation and repression of *Tbx2*. *Development*, **132**(12): 2697–2707.

Singh R, Horsthuis T, Farin HF, et al. 2009. Tbx20 interacts with Smads to confine *Tbx2* expression to the atrioventricular canal. *Circulation Research*, **105**(5): 442–452.

Sowa N, Horie T, Kuwabara Y, et al. 2012. MicroRNA 26b encoded by the intron of small CTD phosphatase (SCP) 1 has an antagonistic effect on its host gene. *Journal of Cellular Biochemistry*, **113**(11): 3455–3465.

Stennard FA, Costa MW, Lai D, et al. 2005. Murine T-box transcription factor Tbx20 acts as a repressor during heart development, and is essential for adult heart integrity, function and adaptation. *Development*, **132**(10): 2451–2462.

Subramanian A, Tamayo P, Mootha VK, et al. 2005. Gene set enrichment analysis: a knowledge-based approach for interpreting genome-wide expression profiles. *Proceedings of the National Academy of Sciences of the United States of America*, **102**(43): 15545–15550.

Takeuchi JK, Lou X, Alexander JM, et al. 2011. Chromatin remodelling complex dosage modulates transcription factor function in heart development. *Nature Communications*, **2**(1): 187.

Truszkowska GT, Bilińska ZT, Muchowicz A, et al. 2017. Homozygous truncating mutation in *NRAP* gene identified by whole exome sequencing in a patient with dilated cardiomyopathy. *Scientific Reports*, **7**(1): 3362.

Tucker NR, Chaffin M, Fleming SJ, et al. 2020. Transcriptional and cellular diversity of the human heart. *Circulation*, **142**(5): 466–482.

VanOudenhove J, Yankee TN, Wilderman A, et al. 2020. Epigenomic and transcriptomic dynamics during human heart organogenesis. *Circulation Research*, **127**(9): e184–e209.

Velayutham N, Alfieri CM, Agnew EJ, et al. 2020. Cardiomyocyte cell cycling, maturation, and growth by multinucleation in postnatal swine. *Journal of Molecular and Cellular Cardiology*, **146**: 95–108.

Wang L, Yu P, Zhou BY, et al. 2020. Single-cell reconstruction of the adult human heart during heart failure and recovery reveals the cellular landscape underlying cardiac function. *Nature Cell Biology*, **22**(1): 108–119.

Wiese C, Grieskamp T, Airik R, et al. 2009. Formation of the sinus node head and differentiation of sinus node myocardium are independently regulated by Tbx18 and Tbx3. *Circulation Research*, **104**(3): 388–397.

Wolf S, Melo D, Garske KM, et al. 2023. Characterizing the landscape of gene expression variance in humans. *PLoS Genetics*, **19**(7): e1010833.

Yang DH, Gomez-Garcia J, Funakoshi S, et al. 2022. Modeling human multi-lineage heart field development with pluripotent stem cells. *Cell Stem Cell*, **29**(9): 1382–1401. e8.

Ye L, D'agostino G, Loo SJ, et al. 2018. Early regenerative capacity in the porcine heart. *Circulation*, **138**(24): 2798–2808.

Yoshida Y, Yamanaka S. 2017. Induced pluripotent stem cells 10 years later: for cardiac applications. *Circulation Research*, **120**(12): 1958–1968.

Zhang HJ, Pei LJ, Ouyang ZH, et al. 2023a. AP-1 activation mediates post-natal cardiomyocyte maturation. *Cardiovascular Research*, **119**(2): 536–550.

Zhang RL, Yang JC, Zhu J, et al. 2009. Depletion of zebrafish Tcap leads to muscular dystrophy via disrupting sarcomere-membrane interaction, not sarcomere assembly. *Human Molecular Genetics*, **18**(21): 4130–4140.

Zhang YH, Li DH, Han RL, et al. 2017. Transcriptome analysis of the pectoral muscles of local chickens and commercial broilers using Ribo-Zero ribonucleic acid sequencing. *PLoS One*, **12**(9): e0184115.

Zhang ZM, Xu KK, Ji LF, et al. 2023b. A novel loss-of-function mutation in NRAP is associated with left ventricular non-compaction cardiomyopathy. *Frontiers in Cardiovascular Medicine*, **10**: 1097957.

Zhao Y, Liang JL, Liu X, et al. 2024. Tcap deficiency impedes striated muscle function and heart regeneration with elevated ROS and autophagy. *Biochimica et Biophysica Acta (BBA) - Molecular Basis of Disease*, **1870**(8): 167485.

Zhou PZ, Zhang Y, Sethi I, et al. 2022. GATA4 regulates developing endocardium through interaction with ETS1. *Circulation Research*, **131**(11): e152–e168.

Zhu WQ, Zhang E, Zhao M, et al. 2018. Regenerative potential of neonatal porcine hearts. *Circulation*, **138**(24): 2809–2816.

Zhu YL, Zhou ZM, Huang T, et al. 2022. Mapping and analysis of a spatiotemporal H3K27ac and gene expression spectrum in pigs. *Science China Life Sciences*, **65**(8): 1517–1534.